Time-of-flight secondary ion mass spectrometry study of zinc carbonation in the presence of stable oxygen-18 and deuterium isotopes

Ville Saarimaa[a*], Aaretti Kaleva[b], Juha-Pekka Nikkanen[b], Erkki Levänen[b], Pasi Väisänen[c], Antti Markkula[c]

[a]Top Analytica, Ruukinkatu 4, FI-20540 Turku, Finland

[b]Materials Science and Environmental Engineering, Tampere University, FI-33101 Tampere, Finland

[c]SSAB Europe, Harvialantie 420, FI-13300 Hämeenlinna, Finland

*Corresponding author. Tel.: +358 44 099 6335. E-mail address:

ville.saarimaa@topanalytica.com

Abstract

Zinc foil was carbonated in supercritical CO_2 in the presence of water containing stable ^{18}O or deuterium isotopes. The carbonation resulted in precipitation of zinc carbonate crystals with hexagonal and cubic morphologies until the source of hydroxyl groups was depleted. Time-of-flight secondary ion mass spectrometry was utilized to map the isotopes in the precipitates. The isotopes were detected in the precipitated structures, which confirms the formation of carbonic acid as the initial corrosion procedure step, followed by zinc dissolution. This finally leads to the arrangement of zinc ions with carbonate ions, and storage of OH-groups between $ZnCO_3$ layers as $Zn(OH)_2$ or molecular water. The results completed chemical composition data obtained with molecular spectroscopy. Mapping of the distribution of hydrogen and oxygen isotopes by ToF-SIMS provided essential information on the reaction routes of carbonation in a humid $scCO_2$ environment.

Keywords: supercritical carbon dioxide, zinc foil, ^{18}O-water, deuterium, ToF-SIMS

Graphical Abstract

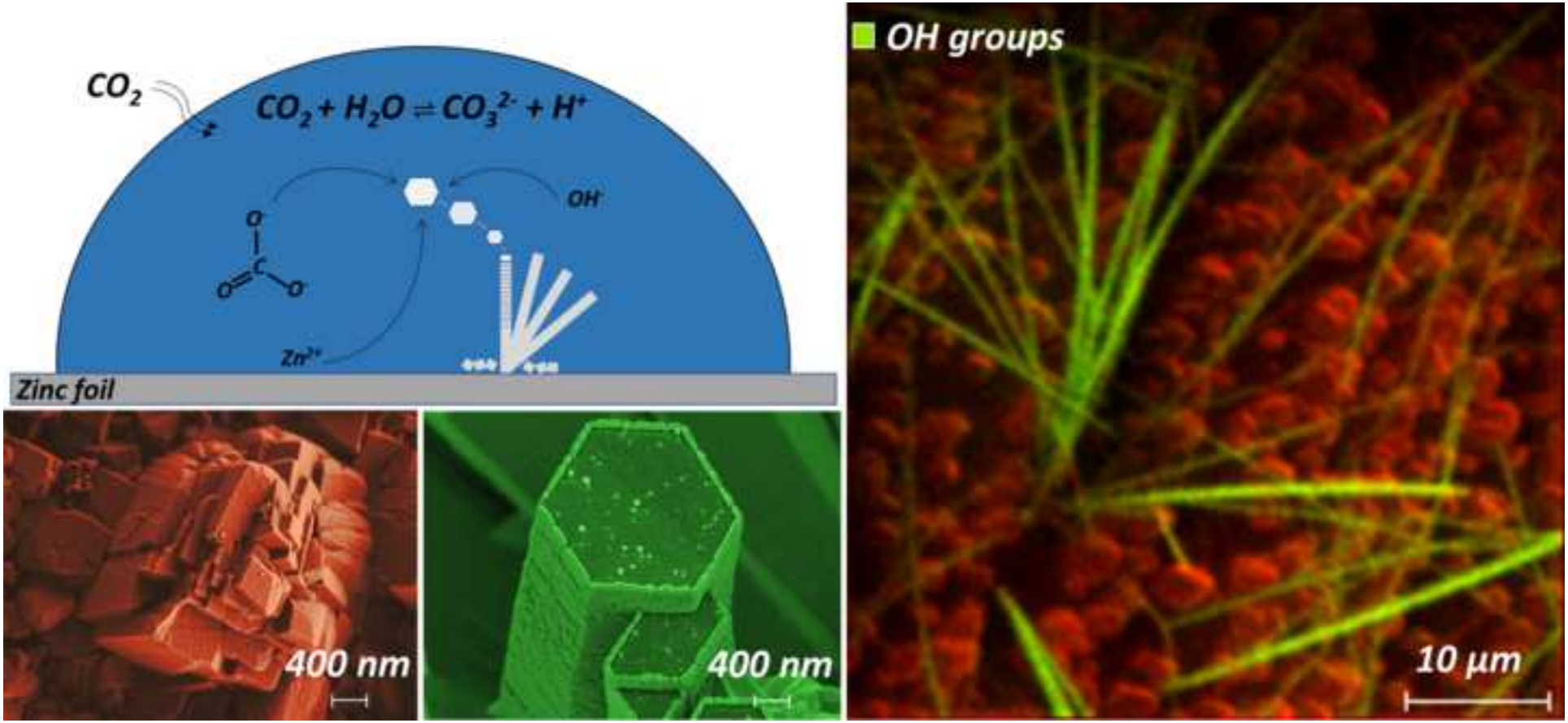

Highlights (for review)

- ^{18}O and deuterium isotopes were used to study reaction routes in humid supercritical carbon dioxide carbonation
- Isotopes in the formed reaction products were mapped by ToF-SIMS
- The presence of hydroxyl groups was unambiguously observed in Zn carbonate nanowires
- Zn carbonate was discerned from zinc hydroxy carbonate by ToF-SIMS mapping of deuterium
- ToF-SIMS is an efficient tool to investigate reaction routes in synthesis of novel nanomaterials

figure1r0.png
Click here to download high resolution image

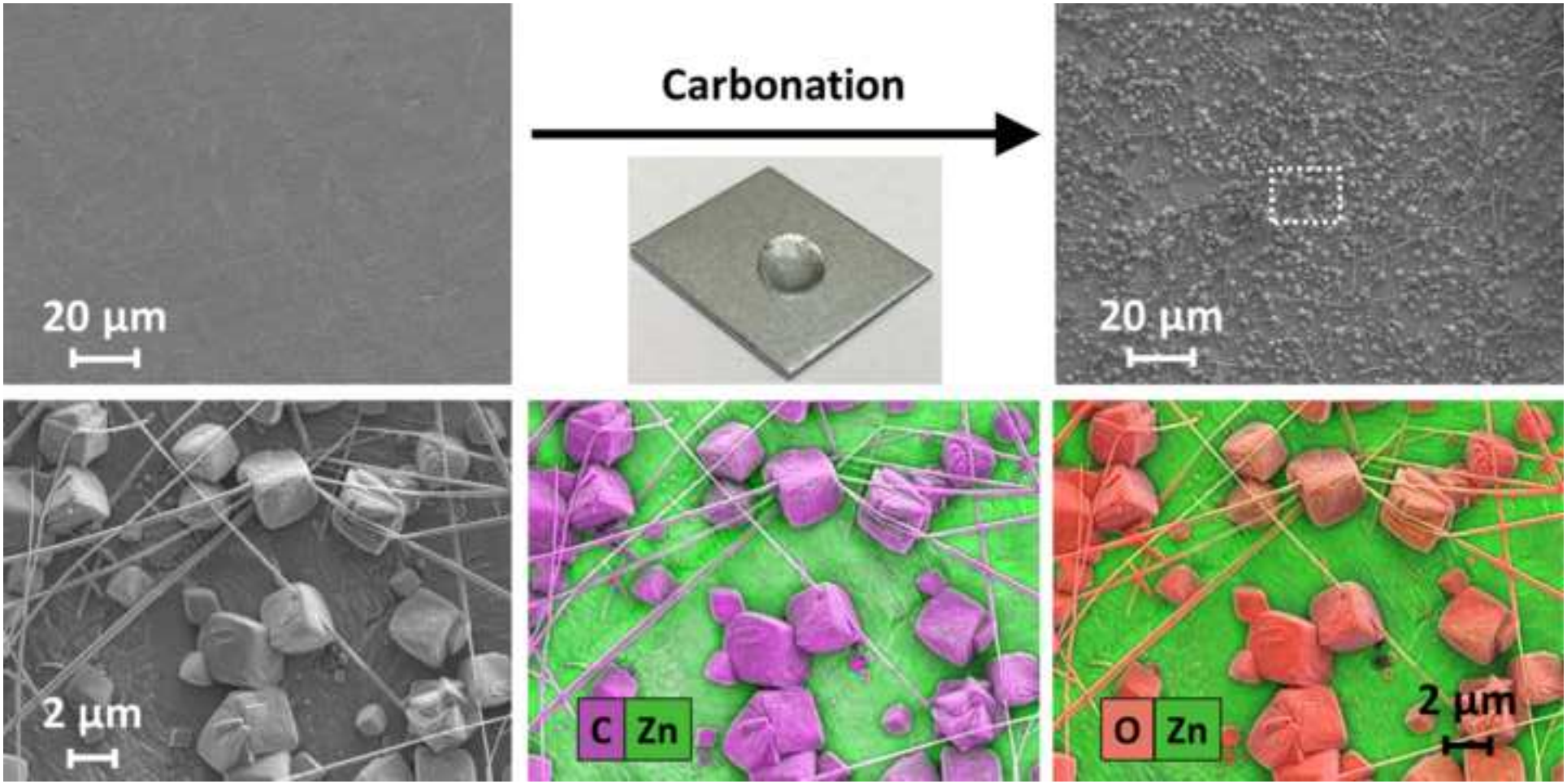

figure2r0.png
Click here to download high resolution image

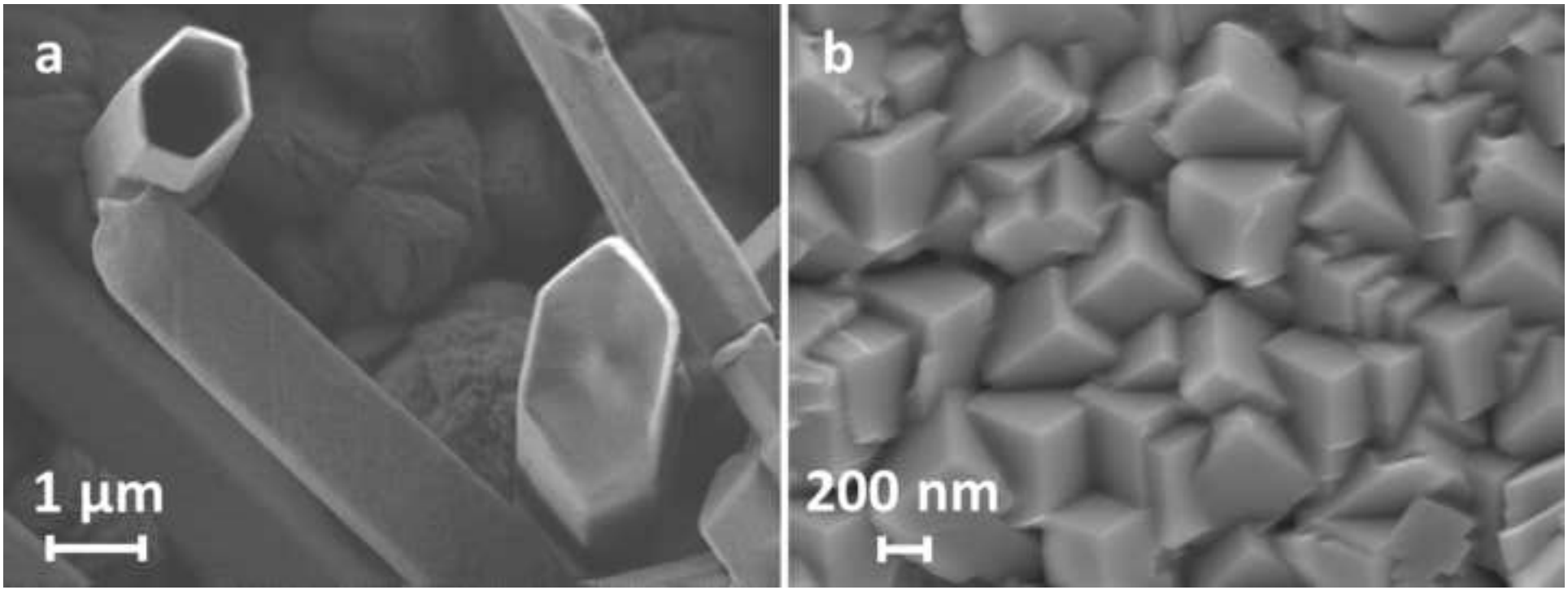

figure3r0.png
Click here to download high resolution image

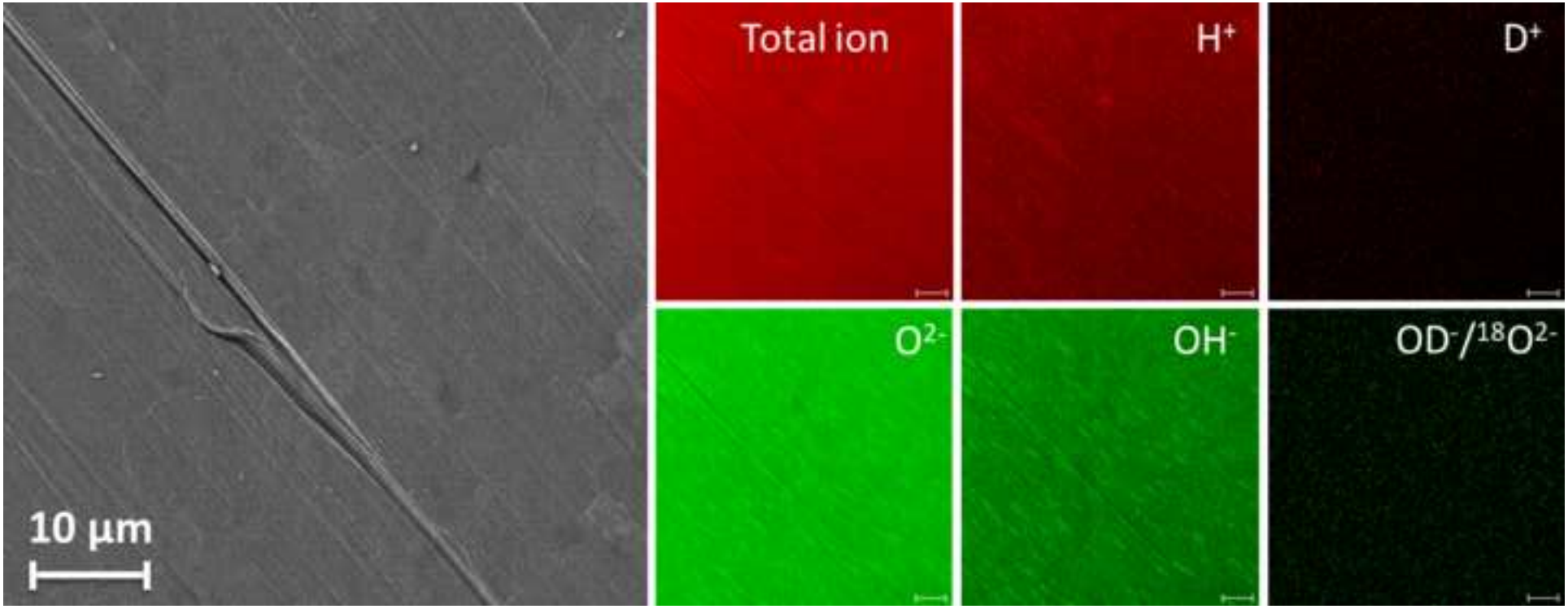

figure4r0.png
Click here to download high resolution image

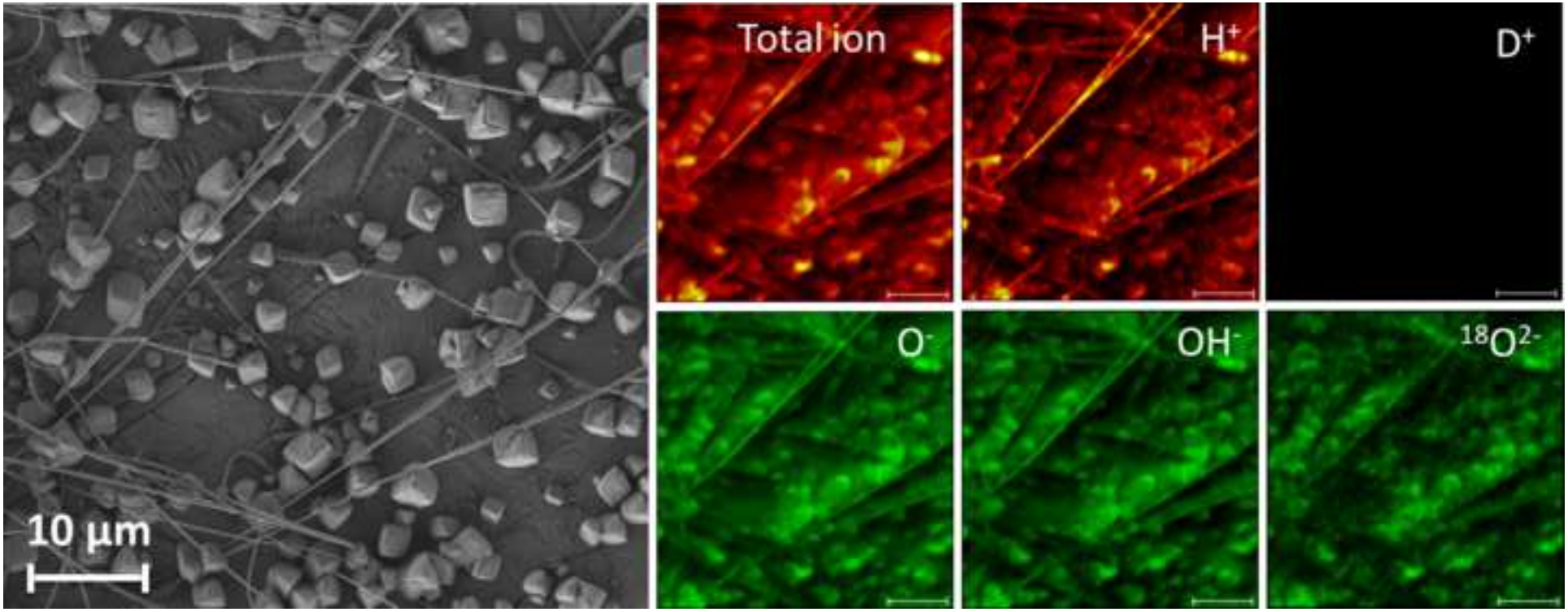

figure5r0.png
Click here to download high resolution image

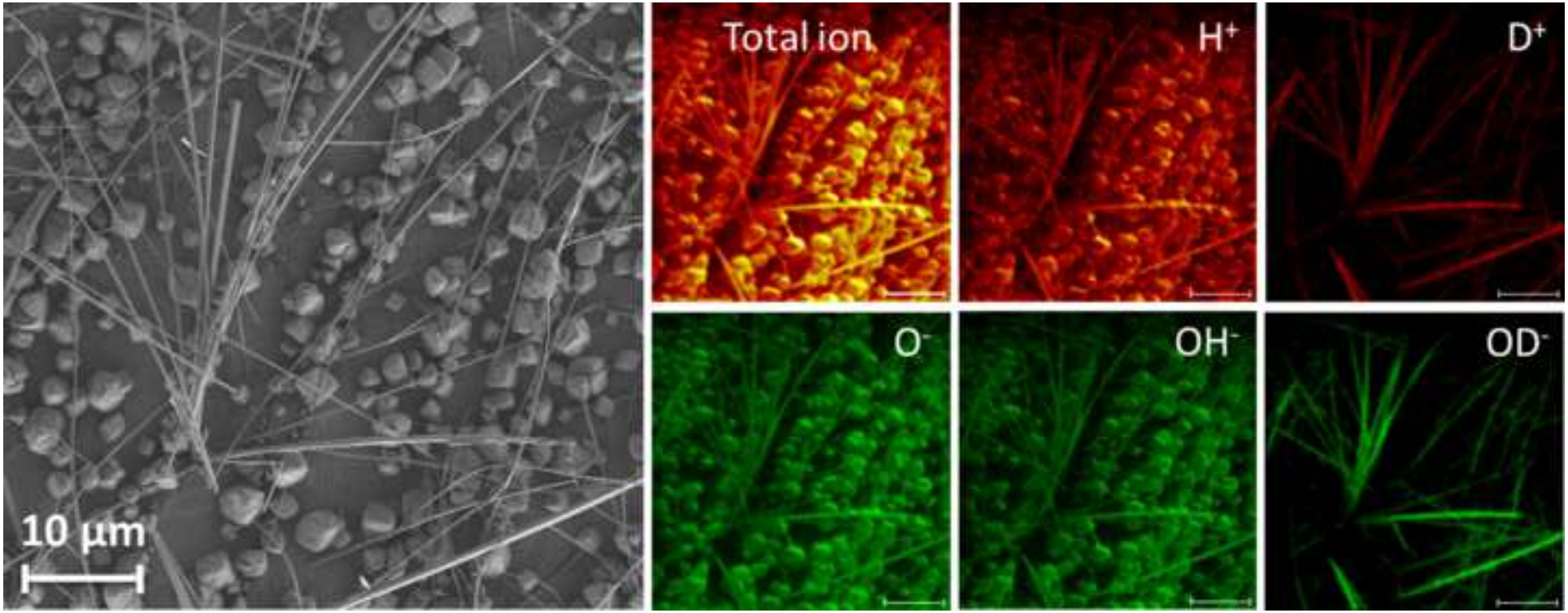

Figure6

Click here to download high resolution image

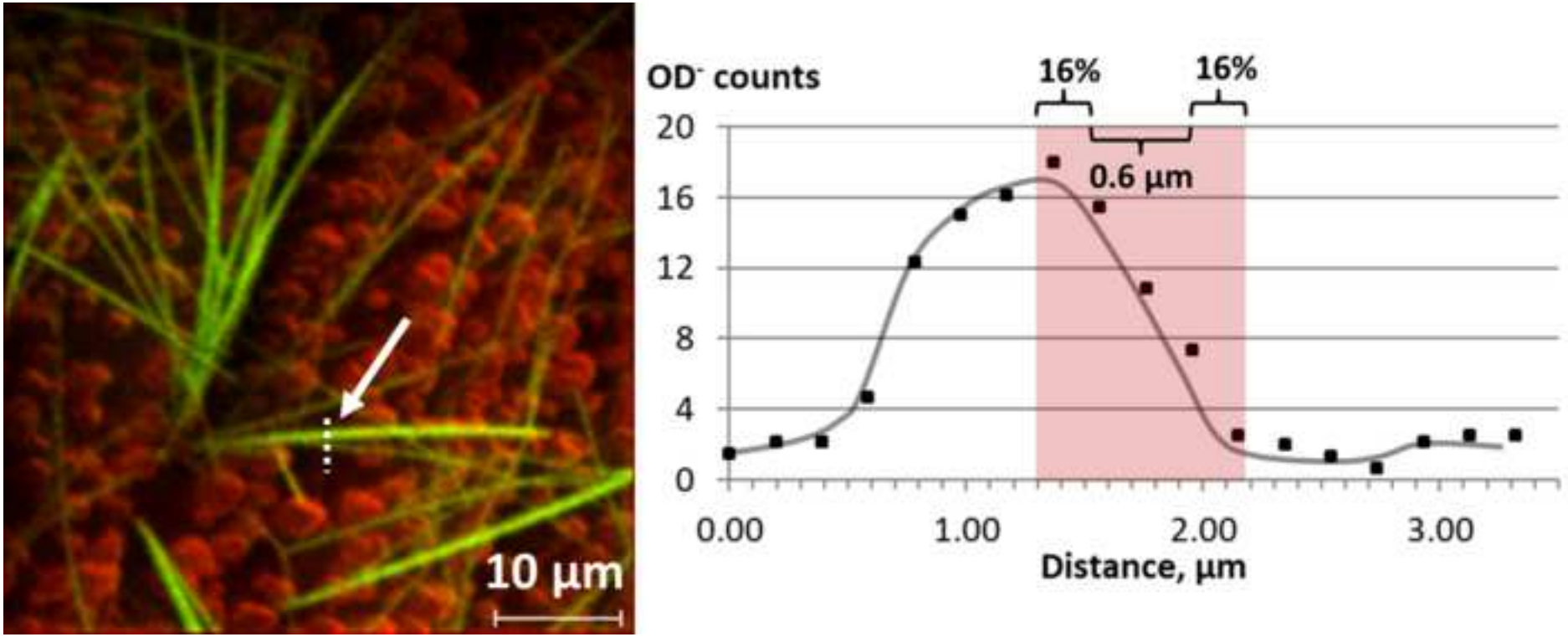

figure7r0.png
Click here to download high resolution image

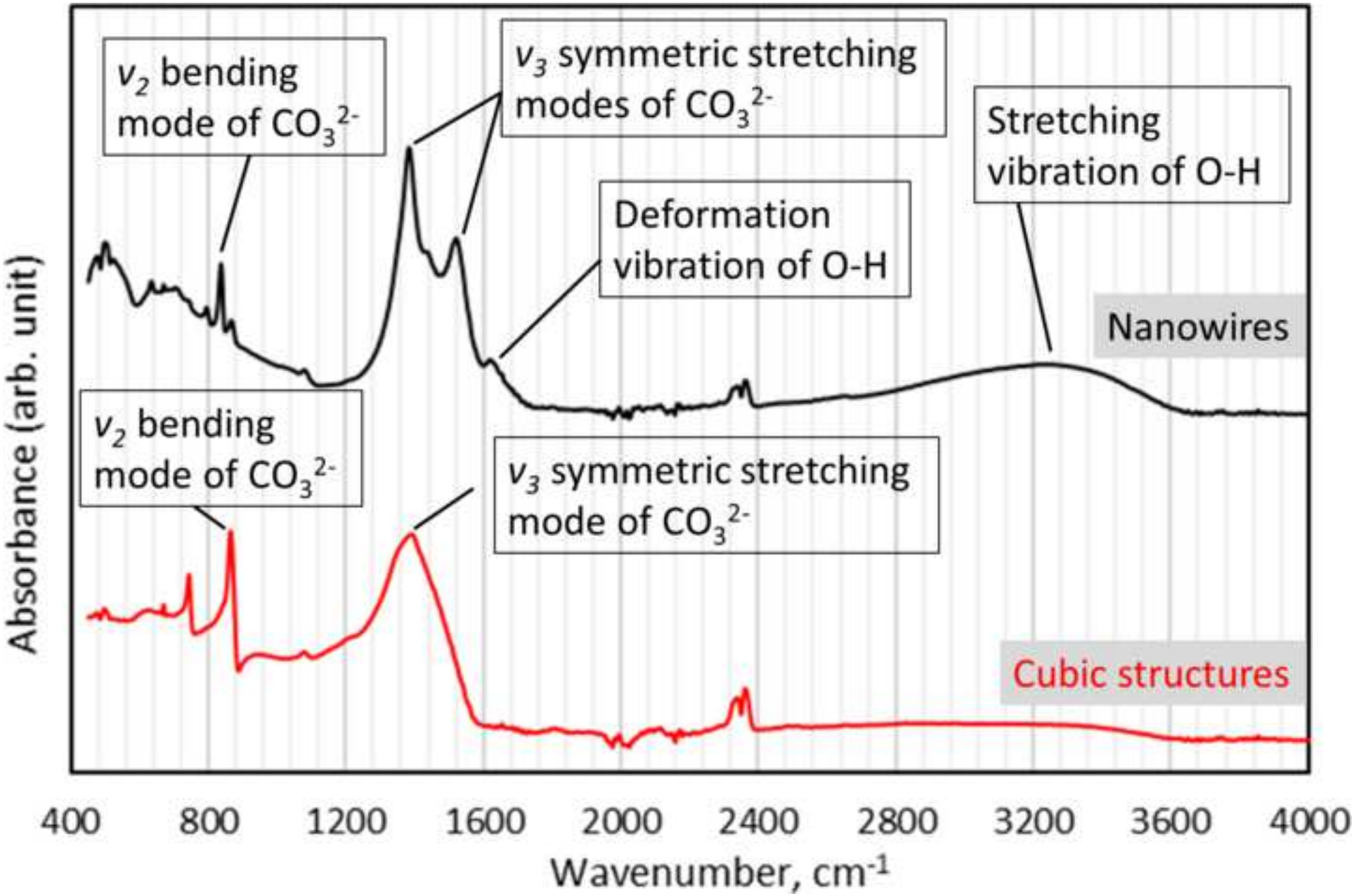

1. Introduction

Metallic zinc is easily oxidized in a humid atmosphere, which results in rapid formation of various simple zinc oxides and hydroxides[1]. These initial zinc corrosion products are in the presence of CO_2 slowly converted into more complex compounds, with basic zinc carbonates ($Zn_x(CO_3)_y(OH)_z$) accounting for most of the species in atmospheres free of contaminants[2]. Compared to salt-induced corrosion processes, carbonation is a slow process[3]. In outdoor exposure, an unprotected zinc substrate receives a carbonated outer layer within some months or years, depending on the local atmosphere, while in laboratory experiments with abundant CO_2 supply the same end products can be formed even in some days or weeks[4,5]. The time required for the formation of stable zinc compounds is further decreased to minutes or hours when a zinc substrate is exposed to humid supercritical carbon dioxide ($scCO_2$)[6]. Contrary to outdoor exposure, $scCO_2$-assisted precipitation of zinc compounds in laboratory produces zinc compounds with a well-defined morphology. The formed precipitates are free of impurities, and such layers are thus suitable for many advanced application areas either as such or as a seed layer for synthetization of functional materials[7–11].

Most of the research related to reactions of metals in humid carbon dioxide-rich environments has been conducted in the area of CO_2 capture plants[12–18], but some similarities can be found in carbonation of minerals[19–23]. It is well known that carbonic acid is formed when water is present in a $scCO_2$ medium ($CO_2 + H_2O \rightleftharpoons H_2CO_3$)[24,25]. Release of ions from a zinc substrate is locally induced by the carbonic acid, and the presence of carbonate ions promotes precipitation of zinc (hydroxy) carbonates that proceeds until the supply of zinc ions and carbonate ions is depleted[6,26–29]. Zinc carbonate and zinc hydroxy carbonate are some of the main reaction products in humid CO_2-assisted zinc carbonation[30]. The reaction steps were recently investigated by ex-situ and in-situ FTIR and Raman measurements[31,32]. In humid $scCO_2$ systems, a thin layer of liquid water is proposed to be present on the corroding surface, allowing interaction of the different ions (Zn^{2+}, OH^-, HCO_3^-, CO_3^{2-})[21,33]. The early corrosion products, that is nanoscale ZnO platforms, serve as initiation points for the carbonate growth[34]. The growth of individual structures is governed by the reaction temperature and pressure. Hydrated metal species are more prone to exchange their OH-groups for carbonate at higher temperature, which favors formation of zinc carbonate (cubic structures)[20,32]. On the contrary, lower

temperatures increase retention of OH-groups, which favors formation of zinc hydroxy carbonate (nanowires). Water is required for formation of both structures. The cubic structures (anhydrous carbonates) are primarily formed at elevated pressure at supercritical state (high amount of dissolved water), while the growth of nanowires (OH-group containing carbonates) is fastest at lower pressure where the capacity of CO_2 to dissolve water is decreased and water is precipitated on the metal surface[34].

However, the presence of hydroxyl groups in the formed precipitates cannot always be completely resolved by molecular spectroscopy[21,35]. Furthermore, the exact reaction routes in various carbonation processes are not yet fully understood. The purpose of this study was to clarify the role of hydroxyl groups in humid scCO_2-assisted carbonation of zinc.

Time-of-flight secondary ion spectroscopy is an important surface sensitive analytical technique capable of distinguishing different ions based on their mass[36–38]. ToF-SIMS has proven efficient in analyzing the chemical composition of corroded surfaces[39–41], and ^{18}O-water and D_2O tracers have been utilized to corrode specimens for specific investigations[42,43]. Although the quantitative accuracy of ToF-SIMS is delimited, the lateral resolution is optimal for mapping of ion fragments in corrosion products[37,43,44]. In addition to corrosion product characterization, ToF-SIMS has been proven efficient in determination of structure and morphology of other nanomaterials[45], and recently in analysis of spatial distribution of components in photoelectrodes[46] and battery materials[47].

In this study, deuterium (^2H) and oxygen-18 (^{18}O) ⁻marked waters were used in scCO_2⁻assisted synthesis of zinc carbonate species on zinc foil, and the presence of these isotopes was mapped in the formed nanostructures.

2. Materials and methods

2.1.Substrate

Zinc foil (0.62 mm thick, 99.9% zinc, Alfa Aesar) was used in all the experiments. The zinc foils were polished in ethanol using SiC paper with grit sizes of 800, 1200, 2000 and 4000. Finally, the samples were cleaned with ethanol and dried.

2.2.H_2O-assisted carbonation

The following isotopes were used: deuterium oxide (D_2O, 99.9 atom-% D, Sigma Aldrich, Canada) and ^{18}O water (≥99 atom-% ^{18}O, Taiyo Nippon Sanso Corporation, Japan). The exposures were carried out by first applying a droplet of water (approx. volume 5 μL) on zinc foil, followed by $scCO_2$ treatment in a batch reactor at 300 bar and 50°C. Then a new droplet of the same water was applied on the same area of zinc, followed by submersion in liquid CO_2, and carbonation at 65 bar and 22°C. In both cases, the treatment was carried out until the water droplets were depleted. The dual exposure was performed to produce two different nanostructures on the same zinc foils[32].

2.3.Surface characterizations

A Zeiss Gemini instrument was employed for SEM imaging of the precipitates. A Bruker QUANTAX FlatQUAD energy dispersive spectrometry (EDS) system was used for element mapping. The signals were collected using a 3 kV accelerating voltage, a 1.2 nA current and a 0.5 μm Mylar window. Time-of-flight secondary ion mass spectroscopy (ToF-SIMS, Phi Trift II) was employed for mapping of ions. The measurements were carried out at 25 kV and 50 μm raster size for a total mapping time of about 1 h. Mild sputtering (30 nC) with Ga^+ ions preceded the measurements. Fourier transform infrared spectroscopy was performed with a Bruker Alpha instrument at 2 cm^{-1} resolution. The measurements were performed in the region 375-4000 cm^{-1} with a single reflection diamond ATR.

3. Results and discussion

3.1. SEM imaging of a carbonated zinc foil

After humid carbonation, two different morphologies were observed on the surface: long nanowires and cubic structures (Fig. 1). The original smooth zinc foil was also visible in the background. The presence of carbon and oxygen was confirmed in both structures by EDS mapping, indicating the presence of carbonate compounds. The close-up images confirm that the zinc carbonate crystals can grow in size in cubic or hexagonal forms that in the literature have been proposed to initiate from small nano-polycrystalline regions on the surface (Fig. 2)[14,17,33,48]. Furthermore, also hollow nanowires were observed, which have not been reported earlier (Fig. 2a).

3.2. ToF-SIMS mapping of carbonated zinc foils

3.2.1. Dry carbonation

SEM image of a zinc foil exposed to dry carbonation, and the ToF-SIMS ion maps from the same area, are shown in Fig. 3. The sample featured a flat, polished surface without visible corrosion products, but with contributions from oxygen and hydroxyl groups evenly scattered across the surface. Adsorption of adventitious atmospheric hydrocarbons and humidity-induced hydroxyl groups onto sample surfaces can result in an increase of apparent surface contamination layer of up to few tens of atom-%[49],[50]. No deuterium or ^{18}O-ions were detected. OD^- and $^{18}O^{2-}$ ions have overlapping masses, but neither fragment was detected, which means that their natural occurrence is very small and that they do not interfere with the experiments with isotope marked waters.

3.2.2. Carbonation in the presence of ^{18}O-water

The presence of ^{18}O-water triggered precipitation of various compounds on the surface (Fig. 4). Zinc carbonate formation has previously been verified in a humid $scCO_2$ atmosphere[6]. In the ToF-SIMS element maps, H^+, O^{2-} and OH^- ions were observed in both morphologies. Within the structures, some local intensity variations were observed that originate in the orientation of the structures related to the incoming ion beam and the detector (shadowing effect). Adsorption of adventitious surface contamination can be assumed to occur for this sample similarly as for the reference sample (Fig. 3) and the distribution of O^{2-} or OH^- ions can be smeared by the potential adsorbed contaminations and were not further examined. No deuterium was detected. $^{18}O^{2-}$ was observed in the precipitates. Formation of carbonic acid is the initial step in zinc carbonation[13,14,51]:

$$CO_2 + H_2O \rightleftharpoons H_2CO_3 \rightleftharpoons H^+ + HCO_3^- \rightleftharpoons H^+ + CO_3^{2-} \quad (1)$$

The presence of carbonic acid triggers zinc dissolution that finally leads to the formation of various zinc carbonate species in conjunction with dissolved zinc and carbonate and hydroxyl groups[14,52–54]:

$$Zn^{2+} + CO_3^{2-} \rightleftharpoons ZnCO_3 \quad (2)$$

$$5Zn^{2+} + 6OH^- + 2CO_3^{2-} \rightleftharpoons Zn_5(OH)_6(CO_3)_2 \quad (3)$$

The occurrence of ^{18}O in the formed precipitates confirms carry-over of ^{18}O species from the water droplet to carbonic acid and ultimately to zinc carbonate precipitates (Fig. 4).

3.2.3. Carbonation in the presence of D_2O

Utilization of deuterium-labeled water in the zinc carbonation enabled detection of hydroxyl groups within the formed corrosion products. In parallel to previous exposures, adventitious O^- and OH^- ions were widely observed, rendering their use in reaction route determination useless (Fig. 5). Importantly, D^+ and OD^- ions showed selective occurrence in the nanowires and were not at all present in the background or the cubic structures. Firstly, this confirms that adsorption of water did not take place during the experiment (adsorbed deuterium-labeled water would be found all over the sample surface). The reactions were continued until the water droplet was depleted, and the introduced water was structurally bonded to the structure. Secondly, the result confirms that the cubic structures did not contain any structural water, but, on the contrary, the nanowires were rich in hydroxyl groups, implying zinc hydroxy carbonate-type precipitates. The obtained lateral resolution (0.6 µm, calculated using the width from 16% to 84% in the line scan[55]) is in line with what has previously obtained for mineral samples with organic phases[43] (Fig. 6).

3.3. Molecular spectroscopy of the precipitates

Composition of zinc carbonate precipitates similar to the ones presented in this study has been previously characterized in the literature. Due to the complexity and the similarity of the precipitates, the compositional data in most reports is tentative[28,48,56,57]. FTIR spectra of the nanowires and the cubic structures are shown in Fig. 7. According to the literature[20,58], the bands at 1380 and 1520 cm^{-1} (nanowires) and the band at 1390 cm^{-1} (cubic structures) arise from the ν_3 symmetric stretching mode of CO_3^{2-}. The ν_2 bending modes of CO_3^{2-} are present at 835 and 860 cm^{-1} (nanowires and cubic structures, respectively)[4,59]. In the nanowire structure, a broad band arising from the stretching vibration of O-H was seen at 2800-3600 cm^{-1}. Hydrogen bonded OH groups that are not coordinately bonded to metal ions cause these stretching modes[50,57]. Furthermore, the absorbance of 1620 cm^{-1} is assigned to the deformation vibration of O-H[20,60]. Associative hydroxyl groups (exhibiting hydrogen bonding) have decreased vibrational energy in comparison with free hydroxyl groups, and the wavenumber shifts to lower

frequency[60]. The presence of OH groups in the nanowire structure, in addition to splitting of the v_3 stretching mode, indicates a hydrozincite-type compound with alternating $Zn(OH)_2$ and $ZnCO_3$ layers, which supports the findings of earlier studies[28,56,61]. A general structure for zinc hydroxy carbonate has been presented as two layers of $ZnCO_3$ fitting between three layers of $Zn(OH)_2$[62]. The structure is linking through two hydroxyl bridges between zinc bound by bidentate of carbonate[60]. Therefore, the coordination number of zinc is four[50]. Water can also be stored between the layers, linked to the complex by hydrogen bonding, the water molecules being located parallel to the carbonate groups that hold the complex zinc-containing sheets together[50,60,62,63]. The $OH:CO_3$ ratio may be variable, resulting in CO_3-deficient, stacking-disordered phases[50]. The results in our earlier studies, obtained with X-ray diffraction (XRD), Raman spectroscopy and X-ray photoelectron spectroscopy (XPS)[32,34], support these findings.

4. Conclusions

Zinc carbonate nanostructures were precipitated on zinc foils by humid carbonation using stable isotope-marked waters (D_2O and $H_2{}^{18}O$) as tracers. The nanostructures grew in hexagonal or cubic forms from singular initiation points until the source of water was depleted. The distribution of the isotopes was successfully mapped by ToF-SIMS, which enabled assessment of reaction routes in the nanostructure synthesis. Growth of nanostructures was not observed in the absence of water. Presence of $^{18}O^{2-}$-ions in the zinc precipitates confirmed the proposed reaction route: $^{18}O^{2-}$-ions were carried over from the ^{18}O-water droplet to carbonic acid ($CO_2 + H_2O \rightleftharpoons H_2CO_3$) and finally to zinc carbonate precipitate ($Zn^{2+} + CO_3^{2-} \rightleftharpoons ZnCO_3$). Further, the use of D_2O revealed that the cubic structures were anhydrous, while the nanowires contained hydroxyl groups. Molecular spectroscopy confirmed the presence of structural hydroxyl groups. Use of isotope-marked water in exposures, combined with ToF-SIMS mapping, is a powerful tool to establish reaction routes and clarify compositions in carbonation of metals and minerals.

References

[1] X.G. Zhang, Corrosion and Electrochemistry of Zinc, 1st ed., Springer Science+Business Media, LCC, New York, 1996.

[2] I. Odnevall, C. Leygraf, Comparison between analytical methods for zinc specimens exposed in a rural atmosphere, J. Electrochem. Soc.D. 138 (1991) 1923–1928.

[3] V. Talakokula, S. Bhalla, R.J. Ball, C.R. Bowen, G.L. Pesce, R. Kurchania, B.

Bhattacharjee, A. Gupta, K. Paine, Diagnosis of carbonation induced corrosion initiation and progression in reinforced concrete structures using piezo-impedance transducers, Sensors Actuators, A Phys. 242 (2016) 79–91. https://doi.org/10.1016/j.sna.2016.02.033.
[4] T. Falk, J. Svensson, L. Johansson, The role of carbon dioxide in the atmospheric corrosion of zinc, J. Electrochem. Soc. 145 (1998) 39–44.
[5] G. Roventi, T. Bellezze, E. Barbaresi, R. Fratesi, Effect of carbonation process on the passivating products of zinc in Ca(OH)2 saturated solution, Mater. Corros. 64 (2013) 1007–1014. https://doi.org/10.1002/maco.201206868.
[6] A. Kaleva, V. Saarimaa, S. Heinonen, J.-P. Nikkanen, A. Markkula, P. Väisänen, E. Levänen, Dissolution-Induced Nanowire Synthesis on Hot-Dip Galvanized Surface in Supercritical Carbon Dioxide, Nanomaterials. 7 (2017) 181–190. https://doi.org/10.3390/nano7070181.
[7] A. Anžlovar, M. Marinšek, Z.C. Orel, M. Žigon, Basic zinc carbonate as a precursor in the solvothermal synthesis of nano-zinc oxide, Mater. Des. 86 (2015) 347–353. https://doi.org/10.1016/j.matdes.2015.07.087.
[8] E. Zehani, S. Hassani, A. Lusson, J. Vigneron, A. Etcheberry, P. Galtier, V. Sallet, Reconstruction of perfect ZnO nanowires facets with high optical quality, Appl. Surf. Sci. 411 (2017) 374–378. https://doi.org/10.1016/j.apsusc.2017.03.201.
[9] G.S. Zakharova, C. Täschner, T. Kolb, C. Jähne, A. Leonhardt, B. Büchner, R. Klingeler, Morphology controlled NH4V3O8 microcrystals by hydrothermal synthesis, Dalt. Trans. 42 (2013) 4897–4902. https://doi.org/10.1039/c3dt32550d.
[10] N. Kanari, D. Mishra, I. Gaballah, B. Dupré, Thermal decomposition of zinc carbonate hydroxide, Thermochim. Acta. 410 (2004) 93–100. https://doi.org/10.1016/S0040-6031(03)00396-4.
[11] S. Heinonen, M. Kannisto, J.P. Nikkanen, E. Huttunen-Saarivirta, M. Karp, E. Levänen, Photocatalytic and antibacterial properties of ZnO films with different surface topographies on stainless steel substrate, Thin Solid Films. 616 (2016) 842–849. https://doi.org/10.1016/j.tsf.2016.10.002.
[12] A. Dugstad, M. Halseid, B. Morland, Testing of CO2 specifications with respect to corrosion and bulk phase reactions, Energy Procedia. 63 (2014) 2547–2556. https://doi.org/10.1016/j.egypro.2014.11.277.
[13] M. Halseid, A. Dugstad, B. Morland, Corrosion and bulk phase reactions in CO2 transport pipelines with impurities: Review of recent published studies, Energy Procedia. 63 (2014) 2557–2569. https://doi.org/10.1016/j.egypro.2014.11.278.
[14] Y. Hua, R. Barker, T. Charpentier, M. Ward, A. Neville, Relating iron carbonate morphology to corrosion characteristics for water-saturated supercritical CO2 systems, J. Supercrit. Fluids. 98 (2015) 183–193. https://doi.org/10.1016/j.supflu.2014.12.009.
[15] Y.S. Choi, S. Nesic, D. Young, Effect of impurities on the corrosion behavior of CO2 transmission pipeline steel in supercritical CO2-water environments, Environ. Sci. Technol. 44 (2010) 9233–9238. https://doi.org/10.1021/es102578c.
[16] T. Nesterova, K. Dam-Johansen, L.T. Pedersen, S. Kiil, Microcapsule-based self-healing anticorrosive coatings: Capsule size, coating formulation, and exposure testing, Prog. Org. Coatings. 75 (2012) 309–318. https://doi.org/10.1016/j.porgcoat.2012.08.002.
[17] Y.-S. Choi, S. Hassani, T.N. Vu, S. Nesic, A.Z.B. Abas, Effect of H2S on the corrosion behavior of pipeline steels in supercritical and liquid CO2 environments, Corrosion. 72 (2015) 999–1009.

[18] B.H. Morland, M. Tjelta, T. Norby, G. Svenningsen, Acid reactions in hub systems consisting of separate non-reactive CO 2 transport lines, Int. J. Greenh. Gas Control. 87 (2019) 246–255. https://doi.org/10.1016/j.ijggc.2019.05.017.
[19] J.S. Loring, J. Chen, P. Bénézeth, O. Qafoku, E.S. Ilton, N.M. Washton, C.J. Thompson, P.F. Martin, B.P. McGrail, K.M. Rosso, A.R. Felmy, H.T. Schaef, Evidence for Carbonate Surface Complexation during Forsterite Carbonation in Wet Supercritical Carbon Dioxide, Langmuir. 31 (2015) 7533–7543. https://doi.org/10.1021/acs.langmuir.5b01052.
[20] J. Loring, C. Thompson, C. Zhang, Z. Wang, H. Schaef, K. Rosso, In situ infrared spectroscopic study of brucite carbonation in dry to water-saturated supercritical carbon dioxide, J. Phys. Chem. A. 116 (2012) 4768–4777.
[21] J. Loring, C. Thompson, Z. Wang, A. Joly, D. Sklarew, H. Schaef, E. Ilton, K. Rosso, A. Felmy, In situ infrared spectroscopic study of forsterite carbonation in wet supercritical CO2, Environ. Sci. Technol. 45 (2011) 6204–6210.
[22] J.H. Kwak, J.Z. Hu, R.V.F. Turcu, K.M. Rosso, E.S. Ilton, C. Wang, J.A. Sears, M.H. Engelhard, A.R. Felmy, D.W. Hoyt, The role of H2O in the carbonation of forsterite in supercritical CO2, Int. J. Greenh. Gas Control. 5 (2011) 1081–1092. https://doi.org/10.1016/j.ijggc.2011.05.013.
[23] A.R. Felmy, O. Qafoku, B.W. Arey, J.Z. Hu, M. Hu, H. Todd Schaef, E.S. Ilton, N.J. Hess, C.I. Pearce, J. Feng, K.M. Rosso, Reaction of water-saturated supercritical CO2 with forsterite: Evidence for magnesite formation at low temperatures, Geochim. Cosmochim. Acta. 91 (2012) 271–282. https://doi.org/10.1016/j.gca.2012.05.026.
[24] A. Davis, B. Oliver, A vibrational-spectroscopic study of the species present in the CO2-H2O system, J. Solut. Chem. 1 (1972) 329–339.
[25] M. O´Connor, A study of the kinetics of the basic zinc carbonate formation reaction, Z. Naturforsch. 30b (1975) 665–668.
[26] G. Patrinoiu, J.M. Calderón-Moreno, D.C. Culita, R. Birjega, R. Ene, O. Carp, Eco-friendly synthetic route for layered zinc compound and its conversion to ZnO with photocatalytical properties, Solid State Sci. 23 (2013) 58–64. https://doi.org/10.1016/j.solidstatesciences.2013.06.011.
[27] E. Diler, B. Lescop, S. Rioual, G. Nguyen Vien, D. Thierry, B. Rouvellou, Initial formation of corrosion products on pure zinc and MgZn2 examinated by XPS, Corros. Sci. 79 (2014) 83–88. https://doi.org/10.1016/j.corsci.2013.10.029.
[28] M. Shamsipur, S.M. Pourmortazavi, S.S. Hajimirsadeghi, M.M. Zahedi, M. Rahimi-Nasrabadi, Facile synthesis of zinc carbonate and zinc oxide nanoparticles via direct carbonation and thermal decomposition, Ceram. Int. 39 (2013) 819–827. https://doi.org/10.1016/j.ceramint.2012.07.003.
[29] Y. Sato, H. Niki, T. Takamura, Effects of Carbonate on the Anodic Dissolution and the Passivation of Zinc Electrode in Concentrated Solution of Potassium Hydroxide, J. Electrochem. Soc. 118 (1971) 1269. https://doi.org/10.1149/1.2408303.
[30] V. Saarimaa, A. Kaleva, J.P. Nikkanen, S. Heinonen, E. Levänen, P. Väisänen, A. Markkula, J. Juhanoja, Supercritical carbon dioxide treatment of hot dip galvanized steel as a surface treatment before coating, Surf. Coatings Technol. 331 (2017) 137–142. https://doi.org/10.1016/j.surfcoat.2017.10.047.
[31] V. Saarimaa, N. Fuertes, D. Persson, T. Zavalis, A. Kaleva, J.-P. Nikkanen, E. Levänen, G. Heydari, Assessment of pitting corrosion in bare and passivated (wet scCO2- induced patination and chemical passivation) hot- dip galvanized steel samples with SVET, FTIR,

and SEM (EDS), Mater. Corros. (2020). https://doi.org/10.1002/maco.202011653.
[32] V. Saarimaa, A. Kaleva, J.-P. Nikkanen, J. Manni, C. Lange, T. Paunikallio, T. Laihinen, S. Heinonen, E. Levänen, P. Väisänen, A. Markkula, Tailoring of Versatile Surface Morphologies on Hot Dip Galvanized Steel in Wet CO2: Aspects on Formation, Barrier Properties, and Utilization as a Substrate for Coatings, ACS Appl. Mater. Interfaces. 10 (2018) 21730–21739. https://doi.org/10.1021/acsami.8b05034.
[33] C.F. Mah, K.P. Beh, F.K. Yam, Z. Hassan, Rapid Formation and Evolution of Anodized-Zn Nanostructures in $NaHCO_3$ Solution, ECS J. Solid State Sci. Technol. 5 (2016) M105–M112. https://doi.org/10.1149/2.0061610jss.
[34] A. Kaleva, T. Tassaing, V. Saarimaa, G. Le Bourdon, P. Väisänen, A. Markkula, E. Levänen, Formation of corrosion products on zinc in wet supercritical and subcritical CO2: In-situ spectroscopic study, Corros. Sci. 174 (2020). https://doi.org/10.1016/j.corsci.2020.108850.
[35] M.C. Hales, R.L. Frost, Synthesis and vibrational spectroscopic characterisation of synthetic hydrozincite and smithsonite, Polyhedron. 26 (2007) 4955–4962. https://doi.org/10.1016/j.poly.2007.07.002.
[36] C.M. Choi, S.J. Lee, J.Y. Baek, J.J. Kim, M.C. Choi, ToF-SIMS analysis of an organic layer using toluene and its cluster ion beam projectiles generated by multiphoton ionization, Appl. Surf. Sci. 458 (2018) 805–809. https://doi.org/10.1016/j.apsusc.2018.07.157.
[37] M. Kubicek, G. Holzlechner, A.K. Opitz, S. Larisegger, H. Hutter, J. Fleig, A novel ToF-SIMS operation mode for sub 100 nm lateral resolution: Application and performance, Appl. Surf. Sci. 289 (2014) 407–416. https://doi.org/10.1016/j.apsusc.2013.10.177.
[38] N. Klingner, R. Heller, G. Hlawacek, S. Facsko, J. von Borany, Time-of-flight secondary ion mass spectrometry in the helium ion microscope, Ultramicroscopy. 198 (2018) 10–17. https://doi.org/10.1016/j.ultramic.2018.12.014.
[39] M. Esmaily, P. Malmberg, M. Shahabi-Navid, J.E. Svensson, L.G. Johansson, A ToF-SIMS investigation of the corrosion behavior of Mg alloy AM50 in atmospheric environments, Appl. Surf. Sci. 360 (2016) 98–106. https://doi.org/10.1016/j.apsusc.2015.11.002.
[40] J. Lehmusto, M. Bergelin, J. Sui, J. Juhanoja, B.J. Skrifvars, P. Yrjas, Applicability of ToF-SIMS and stable oxygen isotopes in KCl-induced corrosion studies at high temperatures, Corros. Sci. 125 (2017) 1–11. https://doi.org/10.1016/j.corsci.2017.05.022.
[41] J. Lehmusto, M. Bergelin, D. Lindberg, J. Juhanoja, The Effect of Oxygen Source on the Reaction Mechanism of Potassium Chloride-Induced High-Temperature Corrosion, Corrosion. 74 (2018) 1431–1445.
[42] K.A. Unocic, H.H. Elsentriecy, M.P. Brady, H.M. Meyer, G.L. Song, M. Fayek, R.A. Meisner, B. Davis, Transmission Electron Microscopy Study of Aqueous Film Formation and Evolution on Magnesium Alloys, J. Electrochem. Soc. 161 (2014) C302–C311. https://doi.org/10.1149/2.024406jes.
[43] M. Senoner, W.E.S. Unger, SIMS imaging of the nanoworld: Applications in science and technology, J. Anal. At. Spectrom. 27 (2012) 1050–1068. https://doi.org/10.1039/c2ja30015j.
[44] E. Deloule, F. Albarède, S.M.F. Sheppard, Hydrogen isotope heterogeneities in the mantle from ion probe analysis of amphiboles from ultramafic rocks, Earth Planet. Sci. Lett. 105 (1991) 543–553. https://doi.org/10.1016/0012-821X(91)90191-J.

[45] N. Perkas, G. Amirian, G. Applerot, E. Efendiev, Y. Kaganovskii, A.V. Ghule, B.-J. Chen, Y.-C. Ling, A. Gedanken, Depositing silver nanoparticles on/in a glass slide by the sonochemical method, Nanotechnology. 19 (2008). https://iopscience.iop.org/article/10.1088/0957-4484/19/43/435604/pdf.
[46] H. Wu, Z. Zheng, C.Y. Toe, X. Wen, J.N. Hart, R. Amal, Y.H. Ng, A pulse electrodeposited amorphous tunnel layer stabilises Cu2O for efficient photoelectrochemical water splitting under visible-light irradiation, J. Mater. Chem. A. 8 (2020) 5638–5646. https://doi.org/10.1039/d0ta00629g.
[47] N. Gauthier, C. Courréges, J. Demeaux, C. Tessier, H. Martinez, Probing the in-depth distribution of organic/inorganic molecular species within the SEI of LTO/NMC and LTO/LMO batteries: A complementary ToF-SIMS and XPS study, Appl. Surf. Sci. 501 (2020) 144266. https://doi.org/10.1016/j.apsusc.2019.144266.
[48] L. Zaraska, K. Mika, K. Syrek, G.D. Sulka, Formation of ZnO nanowires during anodic oxidation of zinc in bicarbonate electrolytes, J. Electroanal. Chem. 801 (2017) 511–520. https://doi.org/10.1016/j.jelechem.2017.08.035.
[49] G.C. Smith, Evaluation of a simple correction for the hydrocarbon contamination layer in quantitative surface analysis by XPS, J. Electron Spectros. Relat. Phenomena. 148 (2005) 21–28. https://doi.org/10.1016/j.elspec.2005.02.004.
[50] S. Ghose, The crystal structure of hydrozincite, Acta Cryst. 17 (1964) 1051–1057.
[51] K. Toews, C. Wai, R. Shroll, pH-defining equilibrium between water and supercritical CO2. Influence on SFE of organics and metal mhelates, Anal. Chem. 67 (1995) 4040–4043.
[52] A.K. Alwan, P.A. Williams, Mineral formation from aqueous solution. Part I. The deposition of hydrozincite, Zn5(OH)6(CO3)2, from natural waters, Transit. Met. Chem. 4 (1979) 128–132. https://doi.org/10.1007/BF00618840.
[53] E. Turianicová, M. Kaňuchová, A. Zorkovská, M. Holub, Z. Bujňáková, E. Dutková, M. Baláž, L. Findoráková, M. Balintová, A. Obut, CO2utilization for fast preparation of nanocrystalline hydrozincite, J. CO2 Util. 16 (2016) 328–335. https://doi.org/10.1016/j.jcou.2016.08.007.
[54] R. Frost, M. Hales, D. Wain, Raman spectroscopy of smithsonite, J. Raman Spectrosc. 39 (2008) 108–114.
[55] T. Sakurada, S. Hashimoto, Y. Tsuchiya, S. Tachibana, M. Suzuki, K. Shimizu, Lateral Resolution of EDX Analysis with Ultra Low Acceleration Voltage SEM, J. Surf. Anal. 12 (2005) 118–121.
[56] D. Miles, P. Cameron, D. Mattia, Hierarchical 3D ZnO nanowire structures via fast anodization of zinc, J. Mater. Chem. A. 3 (2015) 17569–17577.
[57] D. Stoilova, V. Koleva, V. Vassileva, Infrared study of some synthetic phases of malachite (Cu2(OH)2CO3)-hydrozincite (Zn5(OH)6(CO3)2) series, Spectrochim. Acta - Part A Mol. Biomol. Spectrosc. 58 (2002) 2051–2059. https://doi.org/10.1016/S1386-1425(01)00677-1.
[58] M.C. Hales, R.L. Frost, Synthesis and vibrational spectroscopic characterisation of synthetic hydrozincite and smithsonite, Polyhedron. 26 (2007) 4955–4962. https://doi.org/10.1016/j.poly.2007.07.002.
[59] N. LeBozec, D. Thierry, D. Persson, C.K. Riener, G. Luckeneder, Influence of microstructure of zinc-aluminium-magnesium alloy coated steel on the corrosion behavior in outdoor marine atmosphere, Surf. Coatings Technol. 374 (2019) 897–909.

https://doi.org/10.1016/j.surfcoat.2019.06.052.
[60] R. Sako, J. Sakai, Effect of curing temperature on coating structure and corrosion resistance of ammonium zirconium carbonate on galvanized steel surface, Surf. Coatings Technol. 219 (2013) 42–49. https://doi.org/10.1016/j.surfcoat.2012.12.050.
[61] A. Kaleva, J. Nikkanen, S. Heinonen, V. Saarimaa, T. Vuorinen, E. Levänen, Synthesis of ZnO nanowires with supercritical carbon dioxide and post heat treatment, Nanotechnology. 29 (2018) 1–7.
[62] J.L. Jambor, Studies of Basic Copper and Zinc Carbonates: 1-Synthetic Zinc Carbonates and Their Relationship ot Hydrozincite, Can. Mineral. 8 (1964) 92–108.
[63] J.D. Yoo, K. Ogle, P. Volovitch, The effect of synthetic zinc corrosion products on corrosion of electrogalvanized steel: I. Cathodic reactivity under zinc corrosion products, Corros. Sci. 81 (2014) 11–20. https://doi.org/10.1016/j.corsci.2013.11.045.

Figure Captions

Fig. 1. SEM images and EDS element maps of humid carbonation products on a zinc surface.

Fig. 2. Close-up SEM images of nanowires (a) and cubic structures (b).

Figure 3. Ion distributions of a zinc foil exposed to $scCO_2$ in the absence of water.

Figure 4. Ion distributions on $ScCO_2$ treated zinc foil after carbonation in the presence of ^{18}O-water.

Figure 5. Ion distributions on $ScCO_2$ treated zinc foil after carbonation in the presence of D_2O.

Figure 6. Determination of instrument resolution from an individual nanowire (marked with an arrow). The ToF-SIMS element maps is an overlay map of OD^- and total ion signals.

Figure 7. FTIR spectra of the precipitates formed in humid carbonation of zinc.